Vertical Routing of Spinning-Dipole Radiation from a Chiral Metasurface

S. A. Dyakov,[1,*] N. A. Gippius,[1] I. M. Fradkin,[1,2] and S. G. Tikhodeev[3,4]

[1] *Skolkovo Institute of Science and Technology, Nobel Street 3, Moscow 121205, Russia*

[2] *Moscow Institute of Physics and Technology, Institutskiy pereulok 9, Moscow Region 141701, Russia*

[3] *A. M. Prokhorov General Physics Institute, RAS, Vavilova 38, Moscow, 119991, Russia*

[4] *Faculty of Physics, Lomonosov Moscow State University, Moscow 119991, Russia*

(Received 3 April 2020; revised 19 June 2020; accepted 13 July 2020; published 28 August 2020)

We propose a perfect photonic router based on a specially designed chiral bimetasurface membrane for spin-polarized point light sources. Due to the mirror symmetry breaking in the chiral metamembrane, the radiation power flux of the clockwise and counterclockwise spinning dipoles to the opposite sides of the slab becomes different. We show that spinning dipoles in the specially designed chiral D_4-symmetrical bimetasurface membrane can emit light either upward or downward depending on their rotation direction. We attribute this phenomenon to the Fano-resonance effect, which is a result of the guided modes coupling with the far field. We show the advantage of D_4-symmetrical structures for the achievement of 100% routing efficiency. This phenomenon can find applications in spintronics for spin-selective interchip coupling or as a measurement tool of spin polarization in memory cells.

DOI: 10.1103/PhysRevApplied.14.024090

I. INTRODUCTION

The ability to control the polarization-sensitive directivity of light propagation in various photonic structures attracts great interest from researchers due to the opportunities it presents in optoelectronics, quantum information processing, and biosensing. It is important for many applications to engineer and enhance a circular dichroism of chiral photonic structures. At the nanoscale, the degrees of freedom, represented by the orbital angular momentum of the light and its circular polarization, influence each other [1–14]. This phenomenon is referred to as spin-orbit interaction of light and it can bring a wide range of functionalities to optical nanodevices based on chiral light-matter interaction.

Various photonic systems have recently been exploited for directional coupling of light into different optical modes [2,15–28]. For example, one can use hyperbolic metamaterials for polarization-controlled routing of emission from spinning dipoles [18,24], whereas the possibility of separating circularly polarized photons spectrally in a chiral cavity with mirrors made of a hyperbolic metasurface without applying an external magnetic field has been considered in Ref. [21]. Color routing with a specially designed metasurface has been demonstrated in Ref. [22]. The routing of exitonic emission in a diluted-magnetic-semiconductor quantum well in hybrid plasmonic semiconductor structures has been demonstrated in Ref. [23]. As for quantum information, in, e.g., Ref. [15], the authors presented a scheme for interfacing an optically addressed spin qubit to a path-encoded photon using a crossed-waveguide device.

In the above examples, the light routing has been realized mostly inside a planar structure assisted by waveguided modes or surface-plasmon-polariton modes. Subsequent manipulation with these photons will require additional devices, which may impose some limitations on the size and sensitivity of the system. In some applications, e.g., for interchip coupling in spintronics, it would be promising to direct the light emission of spin-polarized light sources to the opposite normals of a planar structure.

To demonstrate the possibility of vertical radiative routing of spin-polarized light sources, we consider a periodic silicon membrane with a chiral morphology (see Fig. 1). It consists of a homogeneous slab of thickness d sandwiched between two photonic crystal slabs of equal thickness h. The upper and lower photonic crystal slabs are mirror symmetric with respect to the vertical mirror plane. We will demonstrate that such a D_4-symmetrical structure can be a perfect photonic router. The spin-polarized light sources are simulated by spinning point dipoles, i.e., by the classical model of radiating molecules or quantum dots undergoing a spin-polarized transition.

*s.dyakov@skoltech.ru

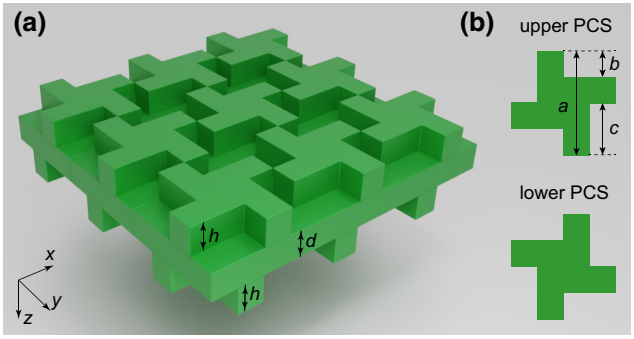

FIG. 1. (a) The schematics of a silicon structure with chiral photonic crystal slabs. The geometrical parameters are $a = 801$ nm, $b = a/4$, $c = a/2$, $h = 686$ nm, and $d = 401$ nm. (b) Unit cells of the upper and lower photonic crystal slabs (PCSs), as seen from the top of the structure.

II. THEORETICAL METHOD

In this work, we use the Fourier modal method in the scattering-matrix form [29] (also known as rigorous coupled-wave analysis [30]) to calculate the optical properties of a chiral metamembrane. The power flow of the dipole's radiation through the horizontal planes at opposite sides of the metamembrane is calculated as a z projection of the Poynting vector integrated over the structure period. In momentum space, it is replaced with summation over the Floquet-Fourier harmonics:

$$P = \frac{c}{16\pi}(E_x^\dagger H_y + E_x H_y^\dagger - E_y^\dagger H_x - E_y H_x^\dagger), \qquad (1)$$

where $E_{x,y}$ and $H_{x,y}$ are the vectors of the Floquet-Fourier components of the x and y projections of the electric and magnetic vectors of the dipole's radiation field, c is the speed of light, and the dagger denotes the conjugate transpose. According to the Fourier-modal-method formalism, $E_{x,y}$ and $H_{x,y}$ are found from the vectors of amplitudes by means of the material matrix $\mathbb{F}$:

$$\begin{bmatrix} E_x \\ E_y \\ H_x \\ H_y \end{bmatrix}_u = \mathbb{F}_u \begin{bmatrix} \vec{o} \\ \vec{u} \end{bmatrix}, \qquad \begin{bmatrix} E_x \\ E_y \\ H_x \\ H_y \end{bmatrix}_d = \mathbb{F}_d \begin{bmatrix} \vec{d} \\ \vec{o} \end{bmatrix}, \qquad (2)$$

where the indices u and d mean that the corresponding quantities are taken in the substrate or superstrate; $\vec{o}$ is a zero vector of the same size as $\vec{u}$ and $\vec{d}$, the outgoing hypervectors, which can be found by the method of oscillating currents [31–36]:

$$\vec{u} = \mathbb{S}_{22}^u \left(\mathbb{S}_{21}^d \mathbb{S}_{12}^u - \mathbb{I}\right)^{-1} \left(\vec{j}_d - \mathbb{S}_{21}^d \vec{j}_u\right), \qquad (3)$$

$$\vec{d} = \mathbb{S}_{11}^d \left(\mathbb{I} - \mathbb{S}_{12}^u \mathbb{S}_{21}^d\right)^{-1} \left(\vec{j}_u - \mathbb{S}_{12}^u \vec{j}_d\right). \qquad (4)$$

In Eqs. (3)–(4), $\mathbb{S}^{u,d}$ are the upper and lower partial scattering matrices [29,34] calculated at a given frequency and emission angle; and $\vec{j}_u$ and $\vec{j}_d$ are the hypervectors of the oscillating dipole's current, which are found from its Floquet-Fourier components J_x, J_y, and J_z by the use of the material matrix $\mathbb{F}$ of the layer where the dipole is located:

$$\begin{bmatrix} \vec{j}_u \\ \vec{j}_d \end{bmatrix} = \mathbb{F}^{-1} \begin{bmatrix} -K_x \tilde{\varepsilon}^{33} J_z/k_0 \\ -K_y \tilde{\varepsilon}^{33} J_z/k_0 \\ -iJ_y + i\tilde{\varepsilon}^{23} J_z \\ +iJ_x - i\tilde{\varepsilon}^{13} J_z \end{bmatrix}. \qquad (5)$$

Here, $\tilde{\varepsilon}$ is the 3×3 block matrix with components that evolve from the Fourier transform of the dielectric permittivity tensor [37], calculated in accordance with Li's factorization rules [38]; $K_{x,y}$ are the diagonal matrices of the x and y components of the photon quasimomentum vector of different diffraction orders; and k_0 is the photon wave number in vacuum.

To simulate the emission of a rotating point dipole positioned at a spatial coordinate $\vec{r}_0$ in terms of the Fourier modal method, we calculate the harmonics of current J_α ($\alpha = x, y, z$) as

$$J_\alpha = j_\alpha e^{-i\vec{r}_0\left(\vec{k}_\parallel + \vec{G}_{mn}\right)}, \qquad (6)$$

where j_α are the components of the current in real space, $\vec{k}_\parallel = \left[k_x, k_y\right]$ is the in-plane wave vector, $\vec{G}_{mn} = [(2\pi m/a), (2\pi n/a)]$ is the basis of vectors in reciprocal space, and m and n are integers. The current is set as $\vec{j} = [1, \pm i, 0]$, where the sign "+" (or "−") corresponds to a counterclockwise (or clockwise) rotating dipole moment seen from the positive z direction. We denote the corresponding dipoles as σ^+ and σ^-, respectively.

In what follows, we normalize the radiation power flux from a dipole in the membrane to the radiation power flux from the same dipole in free space: $I = P/P_0$. We define this ratio as an emissivity.

We use the dielectric permittivity of Si from Ref. [39] (see also Fig. S1 in the Supplemental Material [40]).

III. RESULTS

The calculated normalized emissivity of the σ^+ and σ^- rotating dipoles located in the center of the unit cell of the optimized chiral metamembrane in the up and down directions perpendicular to the structure are shown in Figs. 2(a) and 2(b). Figures 2(c) and 2(d) show the calculated frequency and in-plane-wave-number (in the $\Gamma - X$ and $\Gamma - M$ directions) dependencies of the normalized emissivity $I_{u,d}^{+,-}$ in the up and down directions of the σ^+ or σ^- rotating dipoles, summed over both polarization states

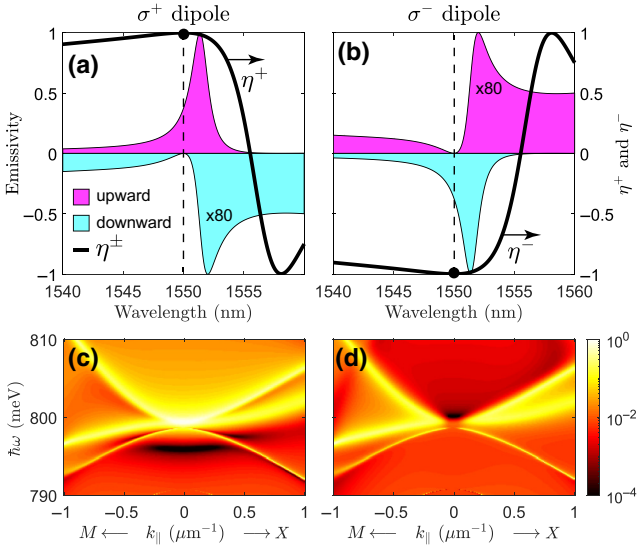

FIG. 2. Normalized emissivity spectra in the up (magenta area) and down (cyan area) directions of (a) σ^+ and (b) σ^- spinning dipoles. The black solid lines denote the corresponding routing efficiencies $\eta^{\pm}$. The in-plane wave number (in the $\Gamma - X$ and $\Gamma - M$ directions) and the frequency dependence of the normalized emissivity of the σ^+ dipole in the vicinity of $\lambda = 1.55\ \mu$m ($\hbar\omega = 800$ meV) in the (c) up and (d) down directions.

of the emitted light. The emissivity of the optimized chiral metamembrane in a wider energy–wave-number range is shown in Fig. S2 of the Supplemental Material [40]. Note that all panels of Fig. 2 show the emissivity, which is normalized to its maximum of approximately 167. This nearly 2-orders-of-magnitude enhancement is due to the Fano-resonance effect discussed below.

Interestingly, the momentum dependence of the downward emissivity near the Γ point in Fig. 2(d) looks very much like the typical behavior of a symmetry-protected bound state in continuum (BIC) (see, e.g., Refs. [41,42] and references therein). However, in our case the emission vanishes in the downward direction only and for the σ^+ dipole, whereas it is open and resonantly enhanced in the opposite upward direction [see Fig. 2(c)]. Correspondingly, there is no shrinking to zero of the resonance line width but only a relative narrowing due to a partial closing of the emission channels. The analogous situation is well known, e.g., for higher resonances at symmetric points of the Brillouin zone, when the symmetry protection works only for highly symmetric directions, whereas the diffraction channels remain open [29].

One can see in Fig. 2 that for both types of dipole, the up and down light emission is different. The structure is optimized so that at a vacuum wavelength of $\lambda = 1.55\ \mu$m, the downward emissivity of the σ^+ dipole is zero, while for the upward direction it is close to the maximum. To describe this asymmetry quantitatively, we introduce the routing efficiencies η^+ and η^-, as well as the total routing efficiency η^{tot}, defined as

$$\eta^{\pm} = \frac{I_u^{\pm} - I_d^{\pm}}{I_u^{\pm} + I_d^{\pm}}, \quad \eta^{\text{tot}} = -\eta^+\eta^-. \tag{7}$$

It becomes possible for the optimized metamembrane to reach $\eta^+ = 1$, $\eta^- = -1$, $\eta^{\text{tot}} = 1$ at $\lambda = 1.55\ \mu$m. Such a perfect routing is due to the vanishing emissivities I_d^+ and I_u^- at this wavelength, this being attributed to the Fano effect. The peaks in Fig. 2 have asymmetric Fano-type shapes; they represent the quasiguided modes (also known as quasinormal guided modes [29,43–50]) that appear in the emission spectra due to the grating-assisted coupling of the emitted light with the photon continuum of the far field [22,29,51–56].

In general, the asymmetric Fano shape appears in the reflection, transmission, or emissivity spectra of a photonic crystal slab as a result of interference of its eigenmode $e(\omega)$, with a smooth background term $b(\omega)$ [44]:

$$x(\omega) = e(\omega) + b(\omega) = \frac{f}{\omega - \omega_0 + i\gamma} + b(\omega), \tag{8}$$

where f is the oscillator strength, ω_0 is the eigenfrequency, and γ is the damping coefficient. In the case of a pure resonance ($b = 0$), the complex-plane trajectory of the parameter $x(\omega)$ is represented by a circle around zero and the emissivity spectrum of $|x(\omega)|^2$ is a symmetric Lorentzian curve. When $b \neq 0$, the spectrum $|x(\omega)|^2$ becomes asymmetric and at certain geometrical parameters and frequencies can be zero. When $b(\omega)$ is a weak function of ω, Eq. (8) is often interpreted as an interference of a discrete state $e(\omega)$ with a continuum of states $b(\omega)$ [53].

Complex-plane diagrams of the x component of the electric field radiated by the σ^+ dipole in the up and down directions are shown in Fig. 3. One can see that the relative phase of E_x changes by the value of 2π with an increase of λ from 1540 nm to 1560 nm. At $\lambda \approx 1550$ nm

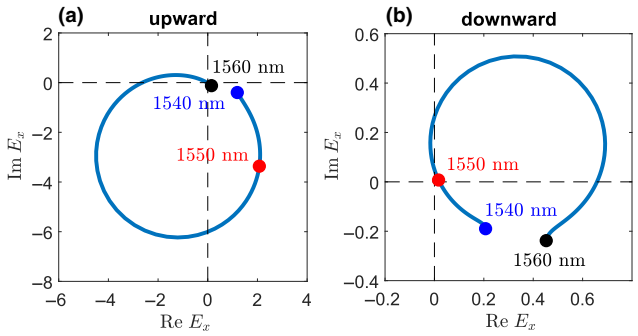

FIG. 3. Complex-plane diagrams of the x component of the electric field radiated by the σ^+ dipole in the (a) up and (b) down directions. The electric field is calculated in the near field of the membrane but only the propagating harmonic is taken into consideration.

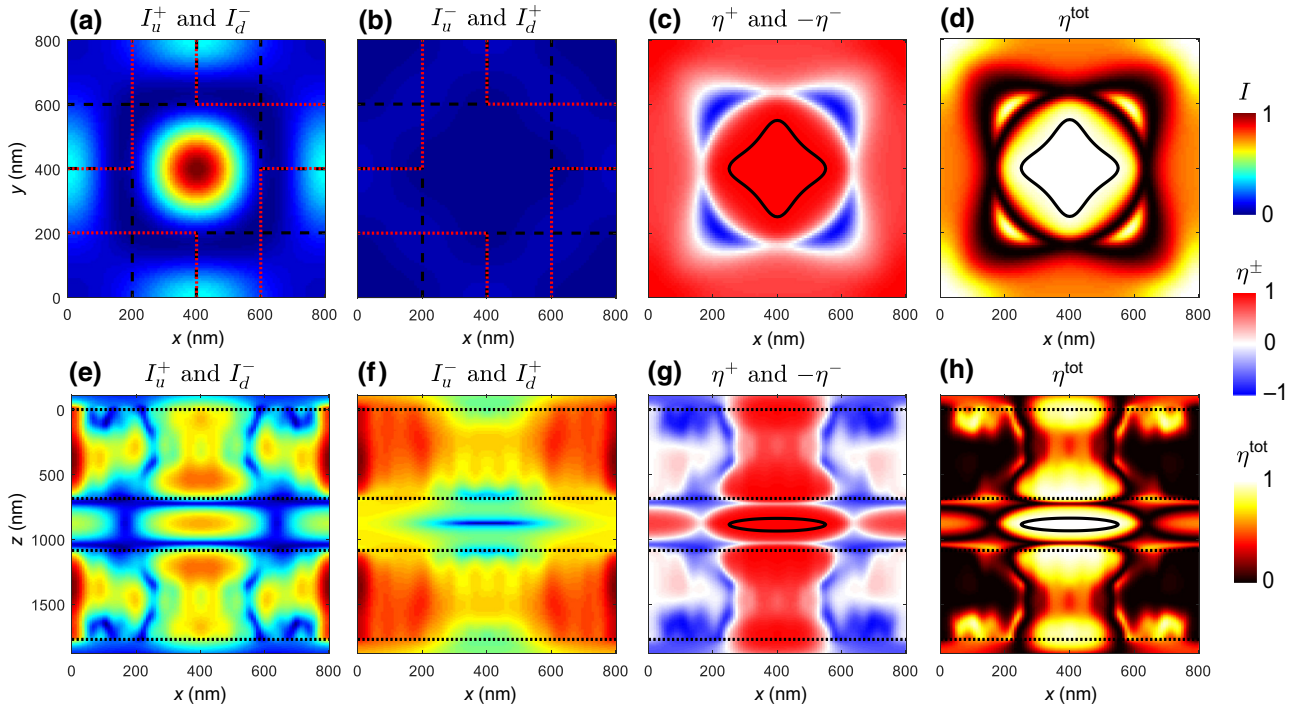

FIG. 4. The dependence of the emissivity (a),(d)–(f) in the up (a),(e) and down (b),(f) directions on the σ^+ dipole's position within an x-y plane (a),(b) and an x-z plane (b),(f), both of which pass through the center of the unit cell. The dependence of the routing efficiency of the σ^+ dipoles (c),(g) and the total routing coefficient (d),(h) on the dipole position. The black dashed and red dotted lines in (a) and (b) show the boundaries of the pillars in the upper and lower photonic crystal slabs. The black dotted lines in (e)–(h) show the boundaries between slabs. The black lines in (c), (d), (g), and (h) bound the regions where $|\eta^{\pm}| > 0.99$. The color scales on the right denote the emissivity, the routing efficiency, and the total routing coefficient.

for downward emission, the phase trajectory of E_x passes through the origin, while for upward emission, the zero point on the phase trajectory is relatively far from the origin. This results in $\eta^{tot} = 1$ at this wavelength. For $\lambda = 1553.6$ nm, the situation is the opposite and $\eta^{tot} = 1$ too. Similar diagrams can be obtained for E_y.

For the practical realization, it is interesting to study the stability of this effect relative to the dipole position. The dependencies of the emissivity in the up and down directions on the σ^+ dipole's position within the horizontal and vertical planes that pass through the center of the cell are shown in Fig. 4. The corresponding dependencies for the σ^- dipoles are the same (not shown); however, one must switch the up and down directions. One can see that these dependencies have maximum and minimum in the central region of the cell. In this region, the emission of the

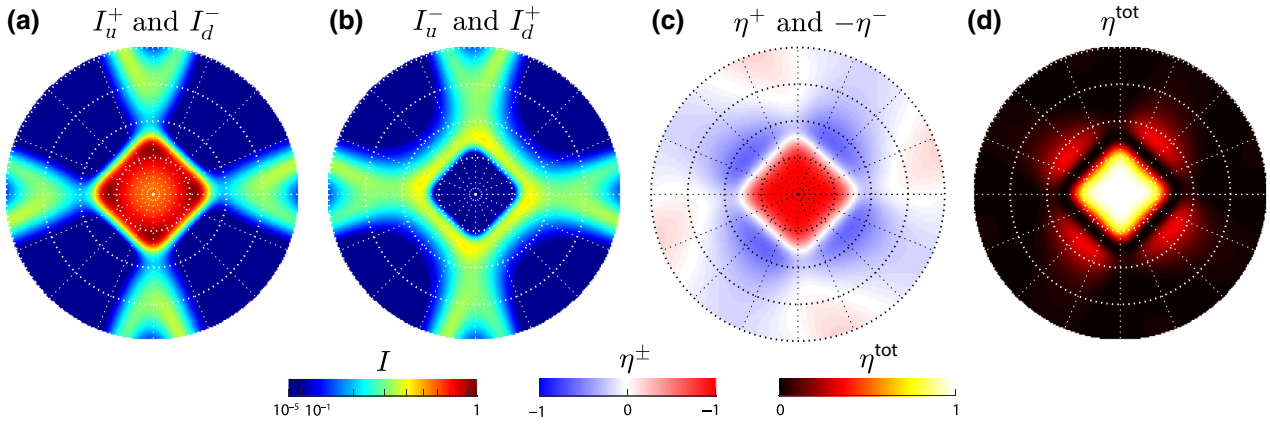

FIG. 5. Angular-emission diagrams within a $\pm 10^\circ$ cone angle of the σ^+ dipoles in the (a) up and (b) down directions: together with (c) the routing coefficient η^+ and (d) the total routing efficiency. The color scale is shown at the bottom.

σ^+ (or σ^-) dipole is not coming out in the downward (or upward) direction and the corresponding routing efficiency is $\eta^+ = 1$ (or $\eta^- = -1$). There are also local minima, from where emission in the up or down directions is sufficiently suppressed; however, the emission is not strictly zero, so that $|\eta^{\pm}| < 1$. The resulting dependencies of the routing efficiencies $\eta^{\pm}$ on the dipole position consist of regions with positive and negative values [Figs. 4(c) and 4(g)]. Figures 4(d) and 4(h) show the total routing efficiency, with the solid lines bounding the regions with $|\eta^{\pm}| > 0.99$. One can see that efficient routing is possible for dipoles located in a rather large volume of the unit cell. If a quantum dot undergoing the spin-polarized transition is placed within this volume, its upward or downward emission will be strongly suppressed.

The angular-emission diagrams of the σ^+ dipoles within the $\pm 10^\circ$ cone are shown in Fig. 5. The lines of high emissivity represent the quasiguided modes of the chiral metamembrane. One can see from Fig. 5 that the effect of routing with $\eta > 0.99$ only exists in the approximately $\pm 2.5^\circ$ cone around the normal angle.

IV. DISCUSSION

In this work, as a proof of principle of routing the emission of spinning dipoles, we use a structure with D_4 rotational symmetry (Fig. 1). Let us now demonstrate that for the effect of perfect routing, D_4 symmetry is more suitable than C_4, which is often used to obtain circular dichroism. The structure shown in Fig. 1 would have C_4 symmetry if it was on the substrate or if it had only one of the chiral photonic crystal slabs.

We start our discussion with C_4-symmetrical structures, as this is a more general case. We consider the electric field generated by an oscillating dipole located in the middle of the cell in the x-y plane at an arbitrary z coordinate. The electric field below and above the membrane is considered. We denote the complex-valued electric field components produced by the x-polarized dipole moment as

$$\vec{E}_u^x = [\alpha, \beta], \quad \vec{E}_d^x = [\rho, \tau]. \tag{9}$$

For the C_4-symmetrical structures, the fields generated by the y-polarized dipole moment have the form

$$\vec{E}_u^y = [-\beta, \alpha], \quad \vec{E}_d^y = [-\tau, \rho]. \tag{10}$$

By the superposition principle, the electric fields from the σ^+ and σ^- polarized dipoles are found as

$$\begin{aligned} \vec{E}_u^{\sigma^\pm} &= \vec{E}_u^x \pm i\vec{E}_u^y = (\alpha \mp i\beta)\,[1, \pm i]\,, \\ \vec{E}_d^{\sigma^\pm} &= \vec{E}_d^x \pm i\vec{E}_d^y = (\rho \mp i\tau)\,[1, \pm i]\,. \end{aligned} \tag{11}$$

With the simultaneous fulfillment of the conditions

$$\alpha = -i\beta, \quad \rho = i\tau, \tag{12}$$

the emission intensities from the σ^+ dipoles in the downward direction and from the σ^- dipoles in the upward direction are zero and the resulting total routing coefficient $\eta^{\text{tot}} = 1$. The electric field components α, β, ρ, and τ depend on the geometrical parameters of the metamembrane and it can be problematic to simultaneously fulfill the above two conditions in structures with C_4 symmetry—whereas D_4-symmetrical structures, such as those shown in Fig. 1, have one more symmetry operation under which the structure is invariant, namely rotation by 180° about the y axis (or, equivalently the x axis). This leads to the fact that a dipole located in the center of the cell of any D_4-symmetrical structure generates an electric field such that $\rho = \alpha$ and $\tau = -\beta$. This makes the conditions (12) equivalent to each other. Thus, for D_4-symmetrical structures, the condition for perfect routing is expressed by only one equality, $\alpha = -i\beta$, which is much easier to satisfy than both of equalities (12) simultaneously (for the dependencies of η^{tot} on the geometrical parameters, see Fig. S3 in the Supplemental Material [40]). Using this condition, we obtain that in D_4-symmetrical structures, the emission from the σ^+ and σ^- dipoles is circularly polarized:

$$\begin{aligned} \vec{E}_u^{\sigma^+} &= [2\alpha, 2i\alpha], \quad \vec{E}_u^{\sigma^-} = [0, 0], \\ \vec{E}_d^{\sigma^+} &= [0, 0], \quad \vec{E}_d^{\sigma^-} = [2\alpha, -2i\alpha]. \end{aligned} \tag{13}$$

From Eq. (13), it follows that the upward emission from the σ^+ dipole and the downward emission from the σ^- dipole both have the same helicity, such that an observer looking in the direction from which the light is coming sees the electric vector rotating counterclockwise sense. By the simultaneous change of the sign of the right-hand side in Eq. (12), one can obtain the condition for the opposite helicity of radiated light: $\alpha = i\beta$. In the described chiral metamembrane, the conditions $\alpha = \mp i\beta$ are fulfilled at $\lambda = 1.55\ \mu$m and $\lambda = 1.5536\ \mu$m, respectively. It is noteworthy that the directions of rotation of the electric vector and the dipole are the same.

In this paper, we consider a metamembrane without absorption losses. It is worth noting that metamembranes with material absorption can also route emission of spin-polarized dipoles with 100% efficiency as long as condition (12) is satisfied. However, the absorption will decrease the far-field emissivity in comparison to lossless structures. This case is considered in greater detail in the Supplemental Material [40] (see Fig. S4).

V. CONCLUSION

In conclusion, we theoretically demonstrate a chiral metamembrane with the highest possible circular dichroism of the light emission of clockwise and counterclockwise rotating electric dipoles. In the structure optimized for optical-communication-wavelength $1.55\ \mu$m, the σ^+ dipole radiates light entirely upward,

while the σ^- dipole radiates entirely downward. We attribute this effect to the appearance of Fano resonance, which occurs due to the grating-assisted coupling of the guided modes with the far field. We show the advantage of the D_4-symmetric structure for the achievement of this effect. This phenomenon can find application in spintronics as a spin-selective photonic router.

ACKNOWLEDGMENTS

This work was supported by the Russian Science Foundation (Grant No. 16-12-10538П). We acknowledge D. A. Gromyko for discussions.

[1] K. Y. Bliokh, F. J. Rodríguez-Fortuño, F. Nori, and A. V. Zayats, Spin-orbit interactions of light, Nat. Photonics **9**, 796 (2015).

[2] P. Lodahl, S. Mahmoodian, S. Stobbe, A. Rauschenbeutel, P. Schneeweiss, J. Volz, H. Pichler, and P. Zoller, Chiral quantum optics, Nature **541**, 473 (2017).

[3] S. A. Dyakov, V. A. Semenenko, N. A. Gippius, and S. G. Tikhodeev, Magnetic field free circularly polarized thermal emission from a chiral metasurface, Phys. Rev. B **98**, 235416 (2018).

[4] S. Dyakov, A. Ignatov, S. Tikhodeev, and N. Gippius, Circularly polarized thermal emission from chiral metasurface in the absence of magnetic field, J. Phys.: Conf. Ser. **1092**, 012028 (2018), IOP Publishing.

[5] N. C. Zambon, P. St-Jean, M. Milićević, A. Lemaître, A. Harouri, L. Le Gratiet, O. Bleu, D. Solnyshkov, G. Malpuech, I. Sagnes, *et al.*, Optically controlling the emission chirality of microlasers, Nat. Photonics **13**, 283 (2019).

[6] S. Tsesses, K. Cohen, E. Ostrovsky, B. Gjonaj, and G. Bartal, Spin-orbit interaction of light in plasmonic lattices, Nano Lett. **19**, 4010 (2019).

[7] P. Woźniak, I. De Leon, K. Höflich, G. Leuchs, and P. Banzer, Interaction of light carrying orbital angular momentum with a chiral dipolar scatterer, Optica **6**, 961 (2019).

[8] S. Zanotto, G. Mazzamuto, F. Riboli, G. Biasiol, G. C. La Rocca, A. Tredicucci, and A. Pitanti, Photonic bands, superchirality, and inverse design of a chiral minimal metasurface, Nanophotonics **8**, 2291 (2019).

[9] K. Y. Bliokh, M. A. Alonso, and M. R. Dennis, Geometric phases in 2D and 3D polarized fields: Geometrical, dynamical, and topological aspects, Rep. Prog. Phys. **82**, 122401 (2019).

[10] Z. Wang, Y. Wang, G. Adamo, J. Teng, and H. Sun, Induced optical chirality and circularly polarized emission from achiral CdSe/ZnS quantum dots via resonantly coupling with plasmonic chiral metasurfaces, Laser Photon. Rev. **13**, 1800276 (2019).

[11] A. Chong, C. Wan, J. Chen, and Q. Zhan, Generation of spatiotemporal optical vortices with controllable transverse orbital angular momentum, Nat. Photonics **14**, 1 (2020).

[12] D. R. Abujetas and J. A. Sánchez-Gil, Spin angular momentum of guided light induced by transverse confinement and intrinsic helicity, ACS Photonics **7**, 534 (2020).

[13] L. Wei and F. J. Rodríguez-Fortuño, Momentum-Space Geometric Structure of Helical Evanescent Waves and its Implications on Near-Field Directionality, Phys. Rev. Appl. **13**, 014008 (2020).

[14] S. Zanotto, A. Tredicucci, D. Navarro-Urrios, M. Cecchini, G. Biasiol, D. Mencarelli, L. Pierantoni, and A. Pitanti, Chiral dielectric metasurfaces: Optomechanics of chiral dielectric metasurfaces (advanced optical materials 4/2020), Adv. Opt. Mater. **8**, 2070016 (2020).

[15] I. J. Luxmoore, N. A. Wasley, A. J. Ramsay, A. C. T. Thijssen, R. Oulton, M. Hugues, S. Kasture, V. G. Achanta, A. M. Fox, and M. S. Skolnick, Interfacing Spins in an InGaAs Quantum Dot to a Semiconductor Waveguide Circuit Using Emitted Photons, Phys. Rev. Lett. **110**, 037402 (2013).

[16] J. Lin, J. P. B. Mueller, Q. Wang, G. Yuan, N. Antoniou, X.-C. Yuan, and F. Capasso, Polarization-controlled tunable directional coupling of surface plasmon polaritons, Science **340**, 331 (2013).

[17] N. Shitrit, I. Yulevich, E. Maguid, D. Ozeri, D. Veksler, V. Kleiner, and E. Hasman, Spin-optical metamaterial route to spin-controlled photonics, Science **340**, 724 (2013).

[18] P. V. Kapitanova, P. Ginzburg, F. J. Rodríguez-Fortuño, D. S. Filonov, P. M. Voroshilov, P. A. Belov, A. N. Poddubny, Y. S. Kivshar, G. A. Wurtz, and A. V. Zayats, Photonic spin Hall effect in hyperbolic metamaterials for polarization-controlled routing of subwavelength modes, Nat. Commun. **5**, 4226 (2014).

[19] J. Petersen, J. Volz, and A. Rauschenbeutel, Chiral nanophotonic waveguide interface based on spin-orbit interaction of light, Science **346**, 67 (2014).

[20] R. Mitsch, C. Sayrin, B. Albrecht, P. Schneeweiss, and A. Rauschenbeutel, Quantum state-controlled directional spontaneous emission of photons into a nanophotonic waveguide, Nat. Commun. **5**, 5713 (2014).

[21] X. Piao, S. Yu, J. Hong, and N. Park, Spectral separation of optical spin based on antisymmetric Fano resonances, Sci. Rep. **5**, 16585 (2015).

[22] C. Yan, K.-Y. Yang, and O. J. Martin, Fano-resonance-assisted metasurface for color routing, Light: Sci. Appl. **6**, e17017 (2017).

[23] F. Spitzer, A. N. Poddubny, I. A. Akimov, V. F. Sapega, L. Klompmaker, L. E. Kreilkamp, L. V. Litvin, R. Jede, G. Karczewski, M. Wiater, T. Wojtowicz, D. R. Yakovlev, and M. Bayer, Routing the emission of a near-surface light source by a magnetic field, Nat. Phys. **14**, 1043 (2018).

[24] W. Liu, V. M. Menon, S. Gao, and G. S. Agarwal, Chiral emission of electric dipoles coupled to optical hyperbolic materials, Phys. Rev. B **100**, 245428 (2019).

[25] I. Fernandez-Corbaton, C. Rockstuhl, P. Ziemke, P. Gumbsch, A. Albiez, R. Schwaiger, T. Frenzel, M. Kadic, and M. Wegener, New twists of 3D chiral metamaterials, Adv. Mater. **31**, 1807742 (2019).

[26] J. Feis, D. Beutel, J. Köpfler, X. Garcia-Santiago, C. Rockstuhl, M. Wegener, and I. Fernandez-Corbaton, Helicity-Preserving Optical Cavity Modes for Enhanced Sensing of Chiral Molecules, Phys. Rev. Lett. **124**, 033201 (2020).

[27] F. Lei, G. Tkachenko, X. Jiang, J. M. Ward, L. Yang, and S. N. Chormaic, Enhanced directional coupling of light

with a whispering gallery microcavity, ACS Photonics **7**, 361 (2020).

[28] I. S. Sinev, F. E. Komissarenko, I. V. Iorsh, D. V. Permyakov, A. K. Samusev, and A. A. Bogdanov, Steering of guided light with dielectric nanoantennas, ACS Photonics **7**, 680 (2020).

[29] S. G. Tikhodeev, A. L. Yablonskii, E. A. Muljarov, N. A. Gippius, and T. Ishihara, Quasiguided modes and optical properties of photonic crystal slabs, Phys. Rev. B **66**, 045102 (2002).

[30] M. Moharam, T. Gaylord, E. B. Grann, and D. A. Pommet, Formulation for stable and efficient implementation of the rigorous coupled-wave analysis of binary gratings, JOSA A **12**, 1068 (1995).

[31] D. M. Whittaker and I. S. Culshaw, Scattering-matrix treatment of patterned multilayer photonic structures, Phys. Rev. B **60**, 2610 (1999).

[32] D. Whittaker, Inhibited emission in photonic woodpile lattices, Opt. Lett. **25**, 779 (2000).

[33] H. Taniyama and M. Notomi, *S*-matrix calculation of radiation characteristics from dipole oscillation in two-dimensional photonic crystal slabs, J. Appl. Phys. **103**, 083115 (2008).

[34] S. V. Lobanov, T. Weiss, D. Dregely, H. Giessen, N. A. Gippius, and S. G. Tikhodeev, Emission properties of an oscillating point dipole from a gold Yagi-Uda nanoantenna array, Phys. Rev. B **85**, 155137 (2012).

[35] I. M. Fradkin, S. A. Dyakov, and N. A. Gippius, Fourier modal method for the description of nanoparticle lattices in the dipole approximation, Phys. Rev. B **99**, 075310 (2019).

[36] I. M. Fradkin, S. A. Dyakov, and N. A. Gippius, Nanoparticle lattices with bases: Fourier modal method and dipole approximation, Phys. Rev. B **102**, 045432 (2020).

[37] T. Weiss, N. A. Gippius, S. G. Tikhodeev, G. Granet, and H. Giessen, Efficient calculation of the optical properties of stacked metamaterials with a Fourier modal method, J. Opt. A **11**, 114019 (2009).

[38] L. Li, New formulation of the Fourier modal method for crossed surface-relief gratings, JOSA A **14**, 2758 (1997).

[39] E. D. Palik and G. Ghosh, *Handbook of Optical Constants of Solids* (Academic Press, New York, 1998), Vol. 3.

[40] See the Supplemental Material at http://link.aps.org/supplemental/10.1103/PhysRevApplied.14.024090 for (i) the wavelength dependence of the dielectric permittivity of the Si used in the Fourier-modal-method simulations; (ii) the emissivity of the optimized chiral metamembrane in a wider energy–wave-number range; (iii) the dependencies of the total routing coefficient on the geometrical parameters of the chiral metamembrane; and (iv) the emissivity of a metamembrane with absorption losses.

[41] Z. F. Sadrieva, M. A. Belyakov, M. A. Balezin, P. V. Kapitanova, E. A. Nenasheva, A. F. Sadreev, and A. A. Bogdanov, Experimental observation of a symmetry-protected bound state in the continuum in a chain of dielectric disks, Phys. Rev. A **99**, 053804 (2019).

[42] S. A. Dyakov, M. V. Stepikhova, A. A. Bogdanov, A. V. Novikov, D. V. Yurasov, Z. F. Krasilnik, S. G. Tikhodeev, and N. A. Gippius, Photonic bound states in the continuum in Si structures with the self-assembled Ge nanoislands, arXiv preprint arXiv:2006.06086 (2020).

[43] P. T. Leung, S. Y. Liu, and K. Young, Completeness and orthogonality of quasinormal modes in leaky optical cavities, Phys. Rev. A **49**, 3057 (1994).

[44] N. A. Gippius, S. G. Tikhodeev, and T. Ishihara, Optical properties of photonic crystal slabs with an asymmetrical unit cell, Phys. Rev. B **72**, 045138 (2005).

[45] E. A. Muljarov, W. Langbein, and R. Zimmermann, Brillouin-Wigner perturbation theory in open electromagnetic systems, EPL **92**, 50010 (2010).

[46] P. T. Kristensen and S. Hughes, Modes and mode volumes of leaky optical cavities and plasmonic nanoresonators, ACS Photonics **1**, 2 (2014).

[47] F. Alpeggiani, N. Parappurath, E. Verhagen, and L. Kuipers, Quasinormal-Mode Expansion of the Scattering Matrix, Phys. Rev. X **7**, 021035 (2017).

[48] E. Lassalle, N. Bonod, T. Durt, and B. Stout, Interplay between spontaneous decay rates and Lamb shifts in open photonic systems, Opt. Lett. **43**, 1950 (2018).

[49] P. Lalanne, W. Yan, A. Gras, C. Sauvan, J.-P. Hugonin, M. Besbes, G. Demésy, M. D. Truong, B. Gralak, F. Zolla, A. Nicolet, F. Binkowski, L. Zschiedrich, S. Burger, J. Zimmerling, R. Remis, P. Urbach, H. T. Liu, and T. Weiss, Quasinormal mode solvers for resonators with dispersive materials, J. Opt. Soc. Am. A **36**, 686 (2019).

[50] A. Gras, W. Yan, and P. Lalanne, Quasinormal-mode analysis of grating spectra at fixed incidence angles, arXiv preprint arXiv:1905.12359 (2019).

[51] U. Fano, The theory of anomalous diffraction gratings and of quasi-stationary waves on metallic surfaces (Sommerfeld's waves), J. Opt. Soc. Am. **31**, 213 (1941).

[52] U. Fano, Effects of configuration interaction on intensities and phase shifts, Phys. Rev. **124**, 1866 (1961).

[53] B. Luk'yanchuk, N. I. Zheludev, S. A. Maier, N. J. Halas, P. Nordlander, H. Giessen, and C. T. Chong, The Fano resonance in plasmonic nanostructures and metamaterials, Nat. Mat. **9**, 707 (2010).

[54] S. A. Dyakov, D. M. Zhigunov, A. Marinins, M. R. Shcherbakov, A. A. Fedyanin, A. S. Vorontsov, P. K. Kashkarov, S. Popov, M. Qiu, M. Zacharias, S. G. Tikhodeev, and N. A. Gippius, Optical properties of silicon nanocrystals covered by periodic array of gold nanowires, Phys. Rev. B **93**, 205413 (2016).

[55] S. A. Dyakov, A. Baldycheva, T. S. Perova, G. V. Li, E. V. Astrova, N. A. Gippius, and S. G. Tikhodeev, Surface states in the optical spectra of two-dimensional photonic crystals with various surface terminations, Phys. Rev. B **86**, 115126 (2012).

[56] S. A. Dyakov, D. M. Zhigunov, A. Marinins, O. A. Shalygina, P. P. Vabishchevich, M. R. Shcherbakov, D. E. Presnov, A. A. Fedyanin, P. K. Kashkarov, S. Popov, *et al.*, Plasmon induced modification of silicon nanocrystals photoluminescence in presence of gold nanostripes, Sci. Rep. **8**, 4911 (2018).